HEAT TRANSFER AND CRITICAL HEAT FLUX OF SUBCOOLED WATER FLOW BOILING IN A SHORT HORIZONTAL TUBE

K. Hata¹, N. Kai², Y. Shirai² and S. Masuzaki³

¹ Institute of Advanced Energy, Kyoto Univ., Gokasho, Uji, Kyoto 611-0011, Japan ² Dept. of Energy Science and Technology, Kyoto Univ., Sakyo-ku, Kyoto 606-8501, Japan ³ National Institute for Fusion Science, 322-6 Oroshi-cho, Toki, Gifu 509-5292, Japan hata@iae.kyoto-u.ac.jp, kai@pe.energy.kyoto-u.ac.jp, shirai@pe.energy.kyoto-u.ac.jp, masuzaki@LHD.nifs.ac.jp

Abstract

The steady-state turbulent heat transfer (THT) due to exponentially increasing heat inputs with various exponential periods ($Q=Q_0exp(t/\tau)$, $\tau=6.55$ to 21.81 s) were systematically measured with the flow velocities, u, of 4.15, 7.05, 10.07 and 13.50 m/s by an experimental water loop flow. Measurements were made on a 6 mm inner diameter, a 59.2 mm effective length and a 0.4 mm thickness of HORIZONTAL Platinum (Pt) circular test tube. The relation between the steady-state turbulent heat transfer and the flow velocity were clarified. The steady state nucleate boiling heat transfer (NBHT) and the steady state critical heat fluxes (CHFs) of the subcooled water flow boiling for HORIZONTAL SUS304 circular test tube were systematically measured with the flow velocities (u=3.94 to 13.86 m/s), the inlet subcoolings ($\Delta T_{sub,in}$ =81.30 to 147.94 K), the inlet pressures (P_{in} =786.29 to 960.93 kPa) and the increasing heat input ($Q_0 \exp(t/\tau)$, τ =8.36 s). The HORIZONTAL SUS304 test tube of inner diameter (d=6 mm), heated length (L=59.4 mm), effective length (L_{eff} =48.4 mm), L/d (=9.9), L_{eff}/d (=8.06) and wall thickness (δ =0.5 mm) with surface roughness (Ra=3.89 μm) was used in this work. The NBHT and the steady state CHFs of the subcooled water flow boiling for the HORIZONTAL SUS304 test tube were clarified at the flow velocities u ranging from 3.94 to 13.86 m/s. The steady-state THT data, the NBHT ones and the steady state CHF ones were compared with the values calculated by authors' THT correlation, their NBHT ones and their transient CHF ones against outlet and inlet subcoolings based on the experimental data for the VERTICAL circular test tubes with the flow velocities u ranging from 4.0 to 42.4 m/s. The influences of test tube orientation on the THT, the NBHT and the subcooled flow boiling CHF are investigated into details and the widely and precisely predictable correlations of the THT, the NBHT and the transient CHFs against outlet and inlet subcoolings in a short HORIZONTAL circular test tube are derived based on the experimental data. The THT correlation, the NBHT ones and the transient CHF ones for the HORIZONTAL test tube can describe the THT data, the NBHT ones and the subcooled flow boiling CHF ones for the wide ranges of $\Delta T_{sub,in}$, u and τ obtained in this work within ± 15 % difference.

Keywords

Turbulent Heat Transfer, Nucleate Boiling Heat Transfer, Critical Heat Flux, Subcooled Water Flow, Short HORIZONTAL Test Tube

1. Introduction

The knowledge of the turbulent heat transfer (THT), the nucleate boiling heat transfer (NBHT) and the critical heat fluxes (CHFs) in subcooled water flow for HORIZONTAL circular test tube is important for the design of a helical type divertor plate in a nuclear fusion facility. The influence of test tube orientation on THT, NBHT and CHF in subcooled water flow will be immediately supposed to be applied to thermal analysis of the divertor of a helical type fusion experimental device which is Large Helical Device (LHD) located in National Institute for Fusion Science (NIFS), Japan. Many researchers have experimentally studied the THT, the NBHT and the steady state CHFs uniformly heated on the VERTICAL circular test tube by a steadily increasing current and given the correlations for calculating THT, NBHT and CHFs on the VERTICAL circular test tube [1-20]. Sawan and Santoro [21] have performed three-dimensional neutronics calculations to determine the detailed spatial distribution of the nuclear parameters in the divertor cassettes used in ITER as shown in Fig. 1. The largest heating and damage occurs in the central dome which has full view of the plasma, not outer vertical target. The power density in the tungsten plasma facing material at the central dome is 16.4 W/cm³. The channel in the central dome is a horizontal orientation.

We have systematically measured the turbulent heat transfer coefficients for the flow velocities (u=4.0 to 21 m/s), the inlet liquid temperatures (T_{in} =296.5 to 353.4 K), the inlet pressures (P_{in} =810 to 1014 kPa) and the increasing heat inputs (Q= $Q_0 exp(t/\tau)$, τ =10, 20 and 33.3 s) by an experimental water loop. The VERTICAL Platinum test tubes of inner diameters (d=3, 6 and 9 mm), heated lengths (L=32.7 to 100 mm), ratios of heated length to inner diameter (L/d=5.51 to 33.3) and wall thickness (δ =0.3, 0.4 and 0.5 mm) with surface roughness (Ra=0.40 to 0.78 μ m) were used. The influence of Reynolds number (Re_d), Prandtl number (Pr), dynamic viscosity (μ_l) and L/d on the turbulent heat transfer was investigated into details and, the widely and precisely predictable correlation of the turbulent heat transfer for heating of water in a short vertical tube was given based on the experimental data [22].

$$Nu_d = 0.02 Re_d^{0.85} Pr^{0.4} \left(\frac{L}{d}\right)^{-0.08} \left(\frac{\mu_l}{\mu_w}\right)^{0.14}$$
 (1)

All properties in the equation are evaluated at the liquid bulk mean temperature, T_{L_2}

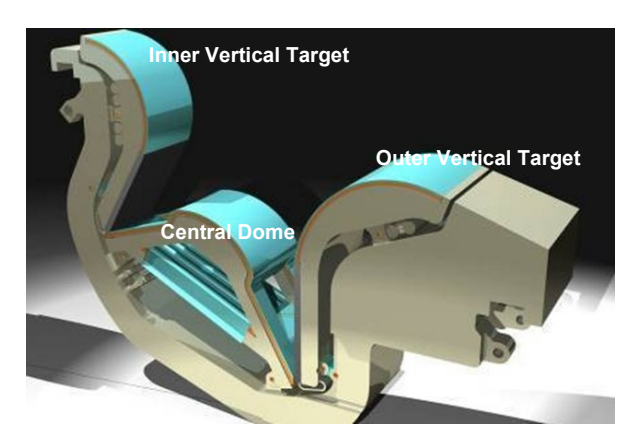


Fig. 1 Three plasma-facing components of ITER divertor (http://www.iter.org/mach/divertor)

[= $(T_{in}+(T_{out})_{cal})/2$], except μ_w , which is evaluated at the heater inner surface temperature. The correlation can describe the turbulent heat transfer coefficients obtained for the wide range of the temperature differences between heater inner surface temperature and liquid bulk mean temperature (ΔT_L =5 to 140 K) with d=3, 6 and 9 mm, L=32.7 to 100 mm and u=4.0 to 21 m/s within ± 15 % difference.

For many years we have already measured the transient CHFs by exponentially increasing heat input $(Q_0 \exp(t/\tau), \tau=16.8 \text{ ms to } 23 \text{ s})$, ramp-wise one $(Q=\alpha t, \alpha=6.21\times10^8 \text{ to } 1.63\times10^{12} \text{ W/m}^3 \text{s})$ and stepwise one $(Q=Q_s, Q_s=2.95\times10^{10} \text{ to } 7.67\times10^{10} \text{ W/m}^3)$ for the VERTICAL SUS304 test tube with the wide range of experimental conditions such as inner diameters (d=2 to 12 mm), heated lengths (L=22 to 149.7 mm), L/d (=4.08 to 74.85), outlet pressures $(P_{out}=159 \text{ kPa to } 1.1 \text{ MPa})$ and flow velocities (u=4.0 to 42.4 m/s) to establish the database for designing the divertor of the LHD [23-38]. And furthermore, we have given the transient CHF correlations against outlet and inlet subcoolings based on the effects of test tube inner diameter (d), flow velocity (u), outlet and inlet subcoolings $(\Delta T_{sub,out}$ and $\Delta T_{sub,in})$, ratio of heated length to inner diameter (L/d) and non-dimensional reduced time, $(\omega_p u/\{\sigma/g/(\rho_l - \rho_g)\}^{0.5})$ on CHF.

Outlet subcooling:

$$Bo = 0.082D^{*-0.1} We^{-0.3} \left(\frac{L}{d}\right)^{-0.1} Sc^{0.7} \times \left(1 + 6.34 t^{*-0.6}\right)$$
for $\Delta T_{sub,out} \ge 30 \text{ K}$ and $u \le 13.3 \text{ m/s}$

$$Bo = 0.0523D^{*-0.15} We^{-0.25} \left(\frac{L}{d}\right)^{-0.1} Sc^{0.7} \times \left(1 + 6.34 t^{*-0.6}\right)$$
for $\Delta T_{sub,out} \ge 30 \text{ K}$ and $u > 13.3 \text{ m/s}$
(3)

Inlet subcooling:

$$Bo = C_1 D^{*-0.1} W e^{-0.3} \left(\frac{L}{d}\right)^{-0.1} e^{-\frac{(L/d)}{C_2 Re_d^{0.4}}} Sc^{*C_3} \times \left(I + 11.4 t^{*-0.6}\right)$$

$$for \ \Delta T_{Sub,in} \ge 40 \text{ K and } u \le 13.3 \text{ m/s}$$

$$Bo = C_4 D^{*-0.15} W e^{-0.25} \left(\frac{L}{d}\right)^{-0.1} e^{-\frac{(L/d)}{C_5 Re^{0.5}}} Sc^{*C_6} \times \left(I + 11.4 t^{*-0.6}\right)$$

$$for \ \Delta T_{Sub,in} \ge 40 \text{ K and } u > 13.3 \text{ m/s}$$
(5)

where C_I =0.082, C_2 =0.53 and C_3 =0.7 for $L/d \le$ around 40 and C_I =0.092, C_2 =0.85 and C_3 =0.9 for $L/d \ge$ around 40. C_4 =0.0523, C_5 =0.144 and C_6 =0.7 for $L/d \le$ around 40 and C_4 =0.0587, C_5 =0.231 and C_6 =0.9 for $L/d \ge$ around 40. Bo, D^* , We, Sc, Sc^* and t^* are boiling number (= $q_{cr,sub}/Gh_{fg}$), non-dimensional diameter [D^* = $d/\{\sigma/g/(\rho_I-\rho_g)\}^{0.5}$], Weber number (= $G^2d/\rho_I\sigma$), non-dimensional outlet subcooling (= $c_{pl}\Delta T_{sub,out}/h_{fg}$), non-dimensional inlet subcooling (Sc^* = $c_{pl}\Delta T_{sub,in}/h_{fg}$) and the non-dimensional reduced time [t^* = $\omega_p u/\{\sigma/g/(\rho_I-\rho_g)\}^{0.5}$] respectively. The reduced times, ω_p , for exponentially increasing heat input, ramp-wise one and stepwise one are τ , $t_{cr}/2$ and t_{cr} , respectively. Saturated thermo-physical properties were evaluated at the outlet pressure. Most of the data for the exponentially increasing heat input (3194 points), the ramp-wise one (208 points) and the stepwise one (105 points) are within ±15 % difference of Eqs. (2), (3), (4) and (5), respectively. Meanwhile, other workers' CHF data [12,15,16] are widely distributed with no

systematic tendency in the whole experimental range, although most of authors' CHF data are within ± 15 % difference of authors' CHF correlations for $\Delta T_{sub,out} \ge 30$ K and $\Delta T_{sub,in} \ge 40$ K.

The objectives of present study are fivefold. First is to measure the THT, the NBHT and the steady state CHFs for HORIZONTAL Pt and SUS304 circular test tubes with wide ranges of inlet subcoolings ($\Delta T_{sub,in}$), flow velocities (u) and exponential periods (τ). Second is to compare with the THT data, the NBHT ones and the steady state CHF ones for the VERTICAL Pt and SUS304 test tubes at the flow velocities u ranging from 4.0 to 13.3 m/s previously obtained. Third is to clarify the influence of test tube orientation on the THT, the NBHT and the subcooled flow boiling CHF. Fourth is to derive the correlations of the THT, the NBHT and the steady state CHF in a short HORIZONTAL test tube based on the experimental data. Fifth is to discuss the mechanism of the THT, the NBHT and the subcooled flow boiling CHF in a short circular test tube.

2. Experimental apparatus and method

The schematic diagram of experimental water loop comprised of the pressurizer is shown in Fig. 2. The loop is made of SUS304 stainless steel and is capable of working up to 2 MPa. The loop has five test sections whose inner diameters are 2, 3, 6, 9 and 12 mm. Test sections were horizontally oriented with water flowing horizontally. The test section of the inner diameter of 6 mm was used in this work. The circulating water was distilled and deionized with about 0.2-µS/cm specific resistivity. The circulating water through the loop was heated or cooled to keep a desired inlet temperature by pre-heater or cooler. The flow velocity was measured by a mass flow meter using a vibration tube (Nitto Seiko, CLEANFLOW 63FS25, Flow range=100 and 750 Kg/min). The flow velocity was controlled by regulating the frequency of the three-phase alternating power source to the multistage canned-type circulation pump with high pump head (Nikkiso Co., Ltd., Non-Seal Pump Multi-stage Type VNH12-C4 C-3S7SP, pump flow rate=12 m³/h, pump head=250 m). The water was pressurized by saturated vapor in the pressurizer in this

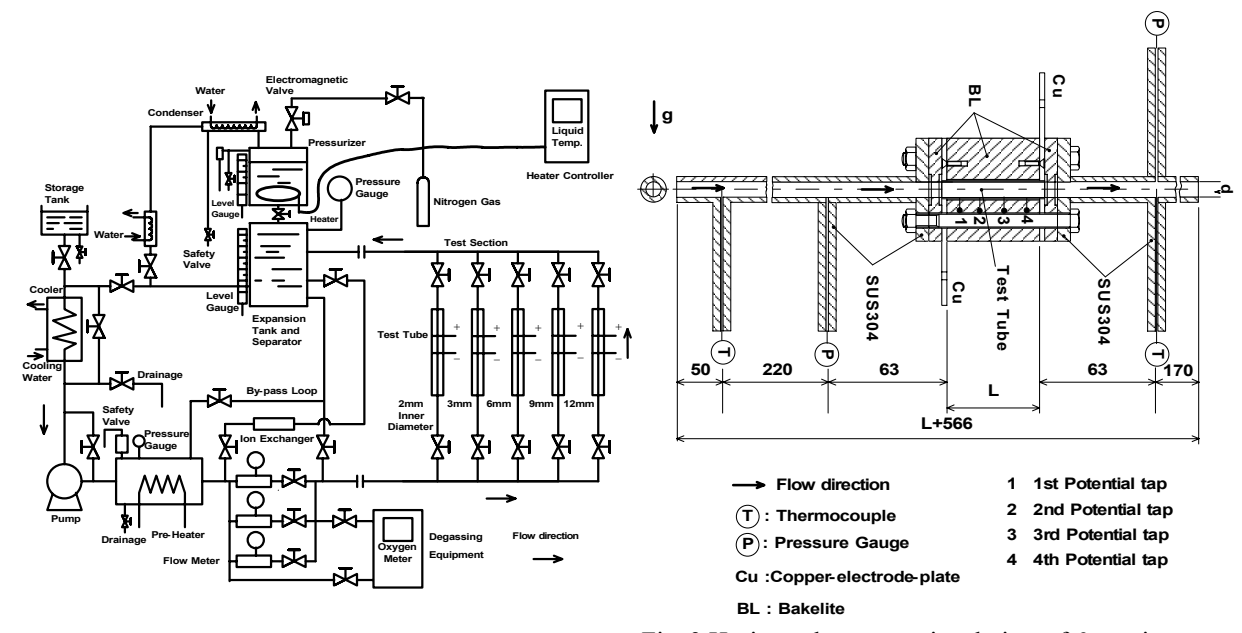


Fig. 2 Schematic diagram of experimental water loop

Fig. 3 Horizontal cross-sectional view of 6-mm inner diameter HORIZONTAL test section

Log Number: 098

work. The pressure at the inlet of the test tube was controlled within ± 1 kPa of a desired value by using a heater controller of the pressurizer.

The cross-sectional view of 6 mm inner diameter HORIZONTAL test section used in this work is shown in Fig. 3. The Platinum (Pt) test tube for the test tube inner diameter, d, of 6 mm, the heated length, L, of 69.6 mm with the commercial finish of inner surface was used for the turbulent heat transfer experiment in this work. Wall thickness of the test tube, δ , was 0.4 mm. The Platinum test tube is highly sensitive for a resistance thermometry. However the CHF data for the wide experimental range could not be obtained. And the SUS304 test tubes with 3 different surface roughness have been generally used for the nucleate boiling heat transfer and CHF experiments. The test tubes with rough and smooth finished inner surfaces (RF and SF) are commercially available. The rough finished inner surface was fabricated by annealing the test tube first in the atmosphere of air and was then acidized, while the smooth finished inner surface was fabricated by annealing the test tube in the atmosphere of hydrogen gas. The smooth finished inner surface test tube was polished up to around 25 µm deep by the electrolytic abrasive treatment to realize the mirror finished one (MF). The rough finished inner surface test tube (RF) was used in this work. Wall thickness of the test tube, δ , was 0.5 mm. Two fine 0.07mm diameter platinum wires were spot-welded on the outer surfaces of the test tubes as potential taps. The effective lengths, L_{eff} , of the Pt and SU304 test tubes between the potential taps on which heat transfer was measured were 59.2 and 48.4 mm, respectively. The silver-coated 5-mm thickness copper-electrode-plates to supply heating current were soldered to the surfaces of the both ends of the test tube. The both ends of test tube were electrically isolated from the loop by Bakelite plates of 14-mm thickness. The inner surface conditions of the test tubes were observed by the scanning electron microscope (SEM) photograph and inner surface roughness was measured by Tokyo Seimitsu Co., Ltd.'s surface texture measuring instrument (SURFCOM 120A). Figure 4 shows the SEM photographs of the Pt and SUS 304 test tubes with the commercial and rough finished inner surfaces (CF and RF). The values of inner surface roughness for Ra, Rmax and Rz were measured 0.45, 2.93 and 1.93 µm for the Pt test tube and 3.89, 21.42 and 15.03 µm for the SUS304 test tube, respectively.

The test tubes have been heated with an exponentially increasing heat input supplied from a direct current source (Takasago Ltd., NL035-500R, DC 35 V- 3000 A) through the two copper electrodes shown in Fig. 5. The value of the initial exponential heat input, Q_0 , was set to be 1.5×10^7 W/m³ throughout the present experiments which was so low that no significant change in heater temperature occurred during the early stage of the run. The common specifications of the direct current source are as follows. Constant-voltage (CV) mode regulation is 0.005 %+3 mV of full scale, CV mode ripple is $500 \mu V$ r.m.s. or better and CV mode transient response time is less than 200 µsec (Typical) against 5 % to full range change of load. The transient CHFs, $q_{cr,sub}$, were realized by the exponentially increasing heat input to the test tube. At the CHF, the test tube average temperature rapidly increases. The current for the heat input to the test tube was automatically cut off when the measured average temperature increased up to the preset temperature, which was several tens of Kelvin higher than corresponding CHF surface temperature. This procedure avoided actual burnout of the test tube.

The transient average temperature of the test tube, \bar{T} , was measured with resistance

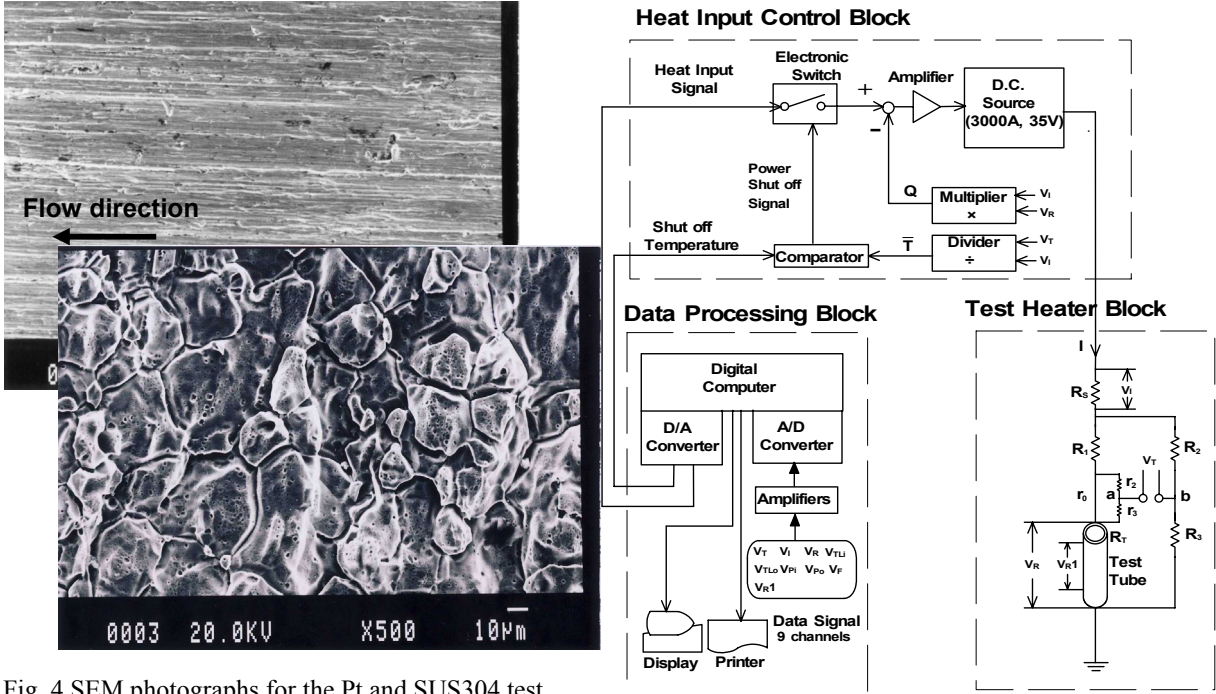


Fig. 4 SEM photographs for the Pt and SUS304 test tubes of *d*=6 mm with the commercial and rough finished inner surfaces.

Fig. 5 Measurement and data processing system

thermometry participating as a branch of a double bridge circuit for the temperature measurement. The output voltages from the bridge circuit, V_T , together with the voltage drops across the two potential taps, V_R , and the two electrodes, V_{RI} , and across a standard resistance, V_I , were amplified and then were sent via a D/A converter to a digital computer. These voltages were simultaneously sampled at a constant interval ranging from 60 to 200 ms. The average temperature of the test tube was calculated with the aid of previously calibrated resistance-temperature relation, $R_T = a(1+b\bar{T}+c\bar{T}^2)$. The heat generation rate in the test tube, Q, was calculated from the measured voltage difference between the potential taps of the test tube and the standard resistance, V_R and V_I . The surface heat flux is the difference between the heat generation rate per unit surface area and the rate of change of energy storage in the test tube obtained from the faired average temperature versus time curve as follows:

$$q(t) = \frac{V}{S} \left(Q(t) - \rho c \frac{d\overline{T}}{dt} \right) \tag{6}$$

where ρ , c, V and S are the density, the specific heat, the volume and the inner surface area of the test tube, respectively. The inner surface temperature, T_s , was also obtained by solving the heat conduction equation in the test tube under the conditions of measured average temperature, \overline{T} , and surface heat flux, q, of the test tube. The temperatures of the heater inner surface, T_s , can be described by the steady one-dimensional heat conduction equation as follows:

$$T_{s} = T(r_{i}) = \overline{T} - \frac{qr_{i}}{4(r_{o}^{2} - r_{i}^{2})^{2} \lambda} \times \left[4r_{o}^{2} \left\{ r_{o}^{2} \left(\ln r_{o} - \frac{1}{2} \right) - r_{i}^{2} \left(\ln r_{i} - \frac{1}{2} \right) \right\} - \left(r_{o}^{4} - r_{i}^{4} \right) \right] - \frac{qr_{i}}{2(r_{o}^{2} - r_{i}^{2}) \lambda} \left(r_{i}^{2} - 2r_{o}^{2} \ln r_{i} \right)$$
 (7)

In case of the 6 mm inner diameter test section, before entering the test tube, the test water flows through the tube with the same inner diameter of the test tube to form the fully developed velocity profile. The entrance tube length, L_e , is given 333 mm ($L_e/d=55.5$). The value of L_e/d for d=6 mm in which the center line velocity reaches 99 % of the maximum value for turbulence flow was obtained ranging from 9.8 to 21.9 by the correlation of Brodkey and Hershey [39] as follows:

$$\frac{L_e}{d} = 0.693 \, Re^{1/4} \tag{8}$$

The inlet and outlet liquid temperatures were measured by 1-mm o.d., sheathed, K-type thermocouples (*Nimblox*, sheath material: SUS316, hot junction: ground, response time (63.2 %): 46.5 ms) which are located at the centerline of the tube at the upper and lower stream points of 283 and 63 mm from the tube inlet and outlet points. The inlet and outlet pressures were measured by the strain gauge transducers (Kyowa Electronic Instruments Co., LTD., PHS-20A, Natural frequency: approximately 30 kHz), which were located near the entrance of conduit at upper and lower stream points of 63 mm from the tube inlet and outlet points. The thermocouples and the transducers were installed in the conduits as shown in Fig. 3. The inlet and outlet pressures were calculated from the pressures measured by inlet and outlet pressure transducers as follows:

$$P_{in} = P_{ipt} - \{ (P_{ipt})_{wnh} - (P_{opt})_{wnh} \} \times \frac{L_{ipt}}{L_{ipt} + L + L_{opt}}$$
(9)

$$P_{out} = P_{in} - \left(P_{in} - P_{opt}\right) \times \frac{L}{L + L_{out}} \tag{10}$$

where L_{ipt} =0.063 m and L_{opt} =0.063 m. Experimental errors are estimated to be ± 1 K in inner tube surface temperature and ± 2 % in heat flux. Inlet flow velocity, inlet and outlet subcoolings, inlet and outlet pressures, and exponential period were measured within the accuracy ± 2 %, ± 1 KPa and ± 2 % respectively.

3. EXPERIMENTAL RESULTS AND DISCUSSION

3.1 Experimental conditions

Steady-state heat transfer processes on the Pt and SUS304 circular test tubes that caused by exponentially increasing heat input, $Q_0 \exp(t/\tau)$, were measured. The exponential periods, τ , of the heat input ranged from 6.55 to 21.81 s. The initial experimental conditions such as inlet flow velocity, inlet subcooling and outlet pressure for the turbulent heat transfer (THT), nucleate boiling heat transfer (NBHT) and CHF experiments were determined independently each other before each experimental run.

The experimental conditions for the THT experiment were as follows:

Heat Input Waveform

Exponentially increasing heat input

Heater material Platinum

Surface condition Commercial finish of inner surface

Surface roughness 0.45 µm for Ra, 2.93 µm for Rmax and 1.93 µm for Rz

Inner diameter (d) 6 mm

Heated length (L) 69.6 mm

Effective Length (L_{eff}) 59.2 mm L/d 11.6 L_{eff}/d 9.87

Wall thickness (δ) 0.4 mm

Inlet flow velocity (u) 4.15, 7.05, 10.07 and 13.50 m/s

Inlet pressure (P_{in}) 818.63 to 853.05 kPa Outlet pressure (P_{out}) 811.46 to 827.19 kPa Inlet subcooling $(\Delta T_{sub,in})$ 145.51 to 148.30 K Outlet subcooling $(\Delta T_{sub,out})$ 138.11 to 142.75 K Inlet liquid temperature (T_{in}) 296.98 to 299.88 K

Increasing heat input (Q) $Q_0 \exp(t/\tau)$, τ =6.55 to 21.81 s

The experimental conditions for the NBHT and CHF experiments were as follows:

Heat Input Waveform Exponentially increasing heat input

Heater Material 304 stainless steel

Surface Condition Rough finished inner surface (commercial finish)

Surface Roughness 3.89 µm for Ra, 21.42 µm for Rmax and 15.03 µm for Rz

Inner Diameter (d) 6 mm Heated Length (L) 59.5 mm Effective Length (L_{eff}) 49.1 mm L/d 9.92 L_{eff}/d 8.18 Wall Thickness (δ) 0.5 mm

Inlet flow velocity (u) 3.93 to 13.86 m/s
Inlet Pressure (P_{in}) 786.29 to 960.93 kPa
Outlet Pressure (P_{out}) 773.41 to 972.00 kPa
Inlet Subcooling ($\Delta T_{sub,in}$) 81.30 to 154.20 K
Outlet Subcooling ($\Delta T_{sub,out}$) 60.40 to 130.30 K
Inlet Liquid Temperature (T_{in}) 297.46 to 362.67 K
Increasing Heat Input (Q) $Q_0 \exp(t/\tau)$, τ =8.36 s

3.2 Steady-state turbulent heat transfer characteristics

Figures 6 and 7 show the typical examples of the steady-state turbulent heat transfer curves for HORIZONTAL Platinum circular tube of d=6 mm and $L_{eff}=59.2$ mm with the exponential periods, τ , of around 22 s at the flow velocities, u, of 4.13 and 13.50 m/s, respectively. The experimental data were compared with the values derived from authors' correlation [22] of the steady-state turbulent heat transfer for the empty tube, Eq. (1), at the flow velocities, u, of 4.13 and 13.50 m/s. The heat fluxes gradually become higher with an increase in the temperature difference between heater inner surface temperature and liquid bulk mean temperature, ΔT_L (= T_s -

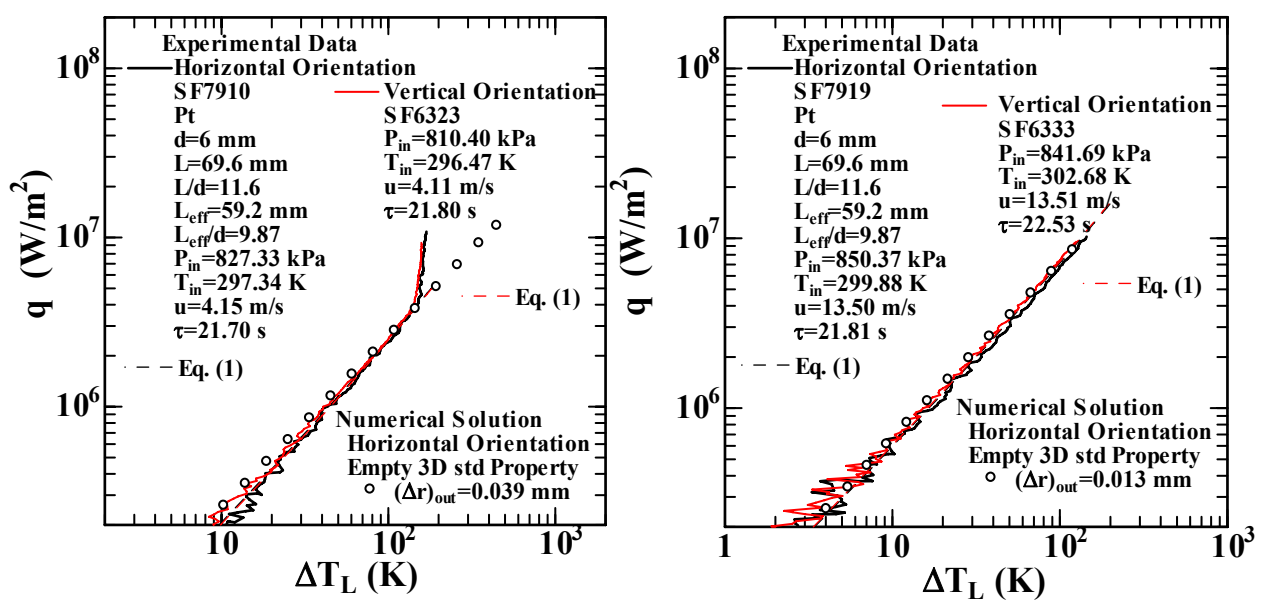


Fig. 6 Relationship between q and ΔT_L [=(T_s - T_L)] for HORIZONTAL Pt circular tube of d=6 mm and L_{eff} =59.2 mm with T_{in} =297.34 K and u=4.15 m/s at P_{in} =827.33 kPa

Fig. 7 Relationship between q and ΔT_L [= $(T_s - T_L)$] for HORIZONTAL Pt circular tube of d=6 mm and L_{eff} =59.2 mm with T_{in} =299.88 K and u=13.50 m/s at P_{in} =850.37 kPa

 T_L), on the steady-state turbulent heat transfer curve derived from Eq. (1). These experimental data are compared with those for the VERTICAL Platinum circular tube shown as red solid lines. The experimental data for the HORIZONTAL and VERTICAL Platinum test tubes as shown in Figs. 6 and 7 show nearly same trend of dependence on the temperature difference between heater inner surface temperature and average bulk liquid temperature, ΔT_L , and the flow velocity, u, for the ΔT_L ranging from 3 to 131 K, although the force of gravity affects the horizontal and vertical velocities of the circulating water through the loop in these experiments respectively.

The experimental results for the HORIZONTAL test tube are compared with the rigorous solutions for the theoretical model of turbulent heat transfer from HORIZONTAL circular tube with a uniform heat flux obtained for the same conditions as the experimental ones considering the temperature dependence of thermo-physical properties by using a commercial CFD cord PHOENICS [40]. Outline of the theoretical equations and calculation method are shown in APPENDIX. Table 1 shows the parameters used for the calculation. The numerical solutions of the HORIZONTAL test tube for the relation between the heat flux, q, and the temperature difference between heater inner surface temperature and average bulk liquid temperature, ΔT_L , are also shown as open circles in Figs. 6 and 7 for the heat flux, q, ranging from 2.55×10^5 to 11.73×10^6 W/m² at the flow velocities of 4.15 and 13.50 m/s. The 14 and 13 different values for the numerical solutions are plotted for the heat flux ranging from 2.55×10^5 to 1.17×10^7 W/m² on the log-log graph. These solutions become also higher with an increase in the ΔT_L along the curve derived from Eq. (1). The numerical solutions solved by the theoretical equations for turbulent heat transfer, Eqs. (19) to (32), in APPENDIX [41] are in good agreement with the experimental data for the HORIZONTAL test tube and the values derived from Eq. (1) within

Table 1 Parameters for calculation

Inner diameter (d) 6 mm Heated length (L)70 mm Entrance length (L_e) 333 mm Exit length (L_{ex}) 33 mm Test section length (L_{ts}) 636 mm 2.55×10^5 to 1.17×10^7 W/m² ($q_0 \exp(t/\tau)$, $\tau = 21.80$ to 22.53 s) Heat flux (q)Inlet flow velocity (*u*) 4.15, 7.12, 10.07 and 13.51 m/s Inlet liquid temperature (T_{in}) 296.47 to 302.68 K Coordinate system Cylindrical coordinate (r, θ, z) Grid number (31 to 35, 60, 978) Physical model K-epsilon model

 ± 10 % difference. The correlation of the steady-state turbulent heat transfer, Eq. (1), can describe the authors' published steady-state turbulent heat transfer data for the VERTICAL test tube with the wide ranges of inlet pressures (P_{in} =810 to 1014 kPa), inner diameters (d=3, 6 and 9 mm), heated lengths (L=32.7 to 100 mm) and flow velocities (u=4.0 to 21 m/s) [22] and those for the HORIZONTAL test tube obtained in this work on d=6 mm and L_{eff} =59.2 mm with L_{eff} /d of 9.87 at the P_{in} =827 to 850 kPa within ± 15 % difference for ΔT_L =3 to 131 K.

3.3 Steady-state nucleate boiling heat transfer

Figure 8 shows the steady-state nucleate boiling heat transfer curves for the exponential period, τ , of around 8.28 s on the HORIZONTAL SUS304 test tube of d=6 mm and L_{eff} =48.4 mm with the rough finished inner surface at the inlet liquid temperatures, T_{in}, of 297.45 to 300.28 K and the flow velocities, u, of 4, 6.9, 9.9 and 13.3 m/s. At the flow velocity of 4 m/s, the heat flux becomes higher with an increase in the surface superheat, ΔT_{sat} (= T_s - T_{sat}), on the non-boiling forced convection curve derived from authors' turbulent heat transfer correlation, Eq. (1), up to the point where the slope begins to increase with heat flux following the onset of nucleate boiling. After that the heat flux increases along the fully developed nucleate boiling curve up to the CHF, at which the transition to film boiling occurs with the rapidly increasing of surface superheat. It is assumed that the transition to film boiling would occur due to the hydro-dynamic instability suggested by Kutateladze [42] and Zuber [43]. At the flow velocities higher than 6.9 m/s, the heat flux gradually becomes higher with an increase in ΔT_{sat} on the non-boiling forced convection curve derived from authors' correlation, Eq. (1), up to the onset of nucleate boiling. After that the slope on the boiling curve does not clearly increase with heat flux even following the onset of nucleate boiling. The CHF and its surface superheat become higher with an increase in flow velocity. The fully developed nucleate boiling curve for the flow velocity of 4 m/s and those for the flow velocity higher than 6.9 m/s almost agree with each other forming straight lines given by Eqs. (11) and (12) on the log q versus $log \Delta T_{sat}$ graph, respectively.

$$q = C\Delta T_{sat}^n = 4.47 \times 10^4 \Delta T_{sat}^{1.5}$$
 for $u=4$ m/s (11)

$$q = 1.11 \times 10^5 \Delta T_{sat}^{1.15}$$
 for $u \ge 6.9 \text{ m/s}$ (12)

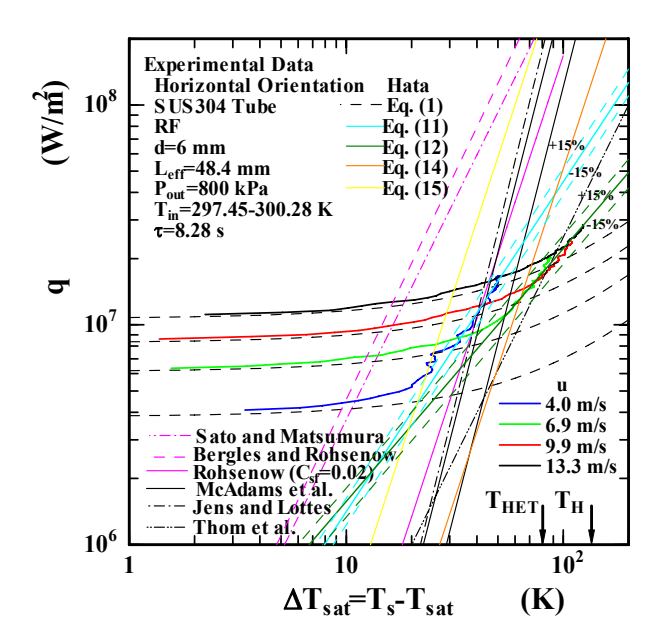


Fig. 8 Typical heat transfer processes on the HORIZONTAL SUS304 test tube of d=6 mm and $L_{eff}=48.4$ mm with the rough finished inner surface for the exponential period of around 8.28 s with the flow velocities of 4.0 to 13.3 m/s

where *C* and *n* are coefficient and exponent.

The equation of incipient boiling superheat given by Bergles and Rohsenow [44] is also shown in the figure for comparison.

$$(\Delta T_{sat})_{ONB} = 0.556 \left(\frac{q}{5.275 P^{1.156}}\right)^{0.4157 P^{0.0234}}$$
(13)

The corresponding curves derived from the correlations for fully developed subcooled boiling in VERTICAL circular tube given by Hata and Masuzaki [35,36,38] are also shown in Fig. 8 for comparison.

$$q = 51.25 \Delta T_{sat}^3$$
 for SUS304 test tubes with the inner surfaces of mirror and rough finished (14)
 $q = 463 \Delta T_{sat}^3$ for Platinum test tube with a commercial finish of inner surface (15)

The corresponding curve derived from the correlation for fully developed subcooled boiling given by Rohsenow [45] are also shown in Fig. 8 for comparison.

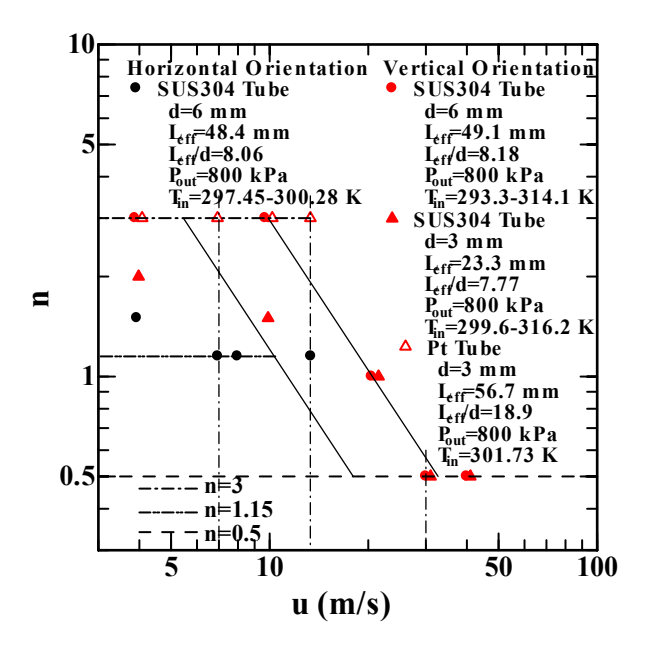
$$\frac{c_{pl}\Delta T_{sat}}{h_{fg}} = C_{sf} \left(\frac{q}{\mu_l h_{fg}} \sqrt{\frac{\sigma}{g(\rho_l - \rho_g)}} \right)^{0.33} \left(\frac{c_{pl} \mu_l}{\lambda_l} \right)^{1.7}$$
(16)

where the various fluid properties are evaluated at the saturation temperature corresponding to the local pressure and C_{sf} is a function of the particular heating surface-fluid combination.

The values of the lower limit of the heterogeneous spontaneous nucleation temperature, T_{HET} , [46] and the homogeneous spontaneous nucleation temperature, T_H , [47] at the pressure of 800 kPa are shown in the figure for comparison. The inner surface temperature of the test tube at CHF for the flow velocity, u, of 13.3 m/s becomes 122.79 K at q=28.50 MW/m², which is 42.36 K higher and 12.36 K lower than the lower limit of the heterogeneous spontaneous nucleation temperature, T_{HET} , and the homogeneous spontaneous nucleation temperature, T_{HET} , respectively.

Figure 9 shows the influence of flow velocity on the exponent, n, of the fully developed nucleate boiling curve and the heat transfer curve up to CHF for the HORIZONTAL SUS304 test tube of d=6 mm and L_{eff} =49.1 mm at inlet liquid temperatures, T_{in} , of 297.45 to 300.28 K. The influence of flow velocity on n for the VERTICAL SUS304 tubes of d=3 mm and L_{eff} =23.3 mm, and d=6 mm and L_{eff} =49.1 mm with the rough finished inner surface [35,38] and the empty Platinum tube of d=3 mm and L_{eff} =56.7 mm with the commercial finish of inner surface [36] at inlet liquid temperatures, T_{in} , of 293.3 to 316.2 K are also shown in the figure for comparison. The values of n for the u ranging from 3.93 to 13.39 m/s and those for the u ranging from 4.0 to 42 m/s were shown versus u with the d and the test tube material as a parameter. The value of n for the HORIZONTAL SUS304 test tube of d=6 mm is almost 1.5 for the u of 3.93 m/s. And those become linearly lower with an increase in the u. That becomes almost about 1.15 at the u of 13.39 m/s.

The effect of flow velocity on the value of ΔT_{sat} (= T_s - T_{sat}) at CHF point, $(\Delta T_{sat})_{cr}$, for HORIZONTAL SUS304 test tube, and that of flow velocity on the $(\Delta T_{sat})_{cr}$ for the VERTICAL SUS304 tubes of d=3 and 6 mm were represented versus the flow velocity, u, in Fig. 10 [35,38]. The $(\Delta T_{sat})_{cr}$ for HORIZONTAL SUS304 test tube become linearly higher with an increase in the flow velocity for the flow velocities ranging from 3.93 to 13.39 m/s, although those for the



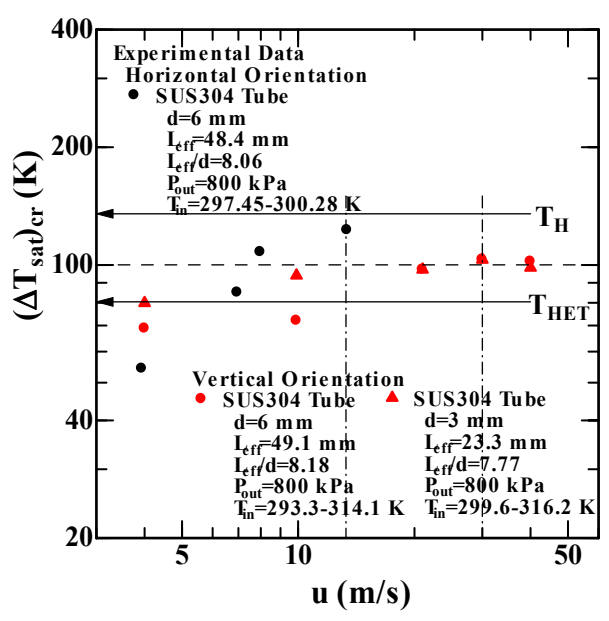


Fig. 9 Values of n versus flow velocity for Horizontal SUS304 test tube and Vertical SUS304 and Pt test tubes.

Fig. 10 Values of ΔT_{sat} at CHF point versus flow velocity for Horizontal SUS304 test tube of d=6 mm and Vertical SUS304 test tubes of d=3 and 6 mm.

VERTICAL SUS304 test tubes of d=3 and 6 mm are almost constant $[(\Delta T_{sat})_{cr}=100 \text{ K}]$ for the u higher than 9.9 m/s. Under the HORIZONTAL test tube, the value of $(\Delta T_{sat})_{cr}$ becomes lower than the VERTICAL test tube at the flow velocity of 3.93 m/s and that becomes higher at the flow velocity of 13.39 m/s. These SUS304 test tubes were not the same serial number but the same manufacturer. It is considered especially in case of HORIZONTAL SUS304 test tube that the heterogeneous spontaneous nucleation temperature would become higher due to a difference between both test tubes. The difference between both surface conditions such as surface roughness and surface wettability would play an important role in nucleate boiling heat transfer.

3.4 Steady-state subcooled flow boiling CHF

3.4.1 Outlet subcooling

Figure 11 shows the steady-state CHFs, $q_{cr,sub,st}$, versus the outlet subcoolings, $\Delta T_{sub,out}$, for the HORIZONTAL SUS304 test tube of the inner diameter (d=6 mm), the heated length (L=59.4 mm), L/d (=9.9) and the wall thickness (δ =0.5 mm) obtained for the flow velocities, u, ranging from 4 to 13.3 m/s at the outlet pressure, P_{out} , of around 800 kPa. The CHF data for the VERTICAL SUS304 test tube of d=6 mm, L=66 mm, L/d =11 and δ =0.5 mm with the flow velocities ranging from 4.0 to 13.3 m/s are also shown in the figure for comparison [23]. As shown in the figure, the $q_{cr,sub,st}$ for each flow velocity become higher with an increase in $\Delta T_{sub,out}$ and the increasing rate becomes lower for higher $\Delta T_{sub,out}$. The CHFs in the whole experimental range become higher with an increase in the flow velocity at a fixed $\Delta T_{sub,out}$.

The curves given by Eq. (2) for the VERTICAL SUS304 test tube are shown in Fig. 11 at each flow velocity for comparison. The CHF data for $\Delta T_{sub,out} \ge 30$ K are in good agreement with the values given by the correlation. Equation (2) was derived based on the experimental data for the VERTICAL SUS304 test tube with the flow velocity ranging from 4 to 13.3 m/s. To confirm the applicability of Eq. (2) to the data for the flow velocity of 4 to 13.3 m/s, the ratios of these CHF data to the corresponding values calculated by Eq. (2) are shown versus $\Delta T_{sub,out}$ in Fig. 12. Most of the data for the HORIZONTAL test tube (69 points) and the VERTICAL one (110 points) are

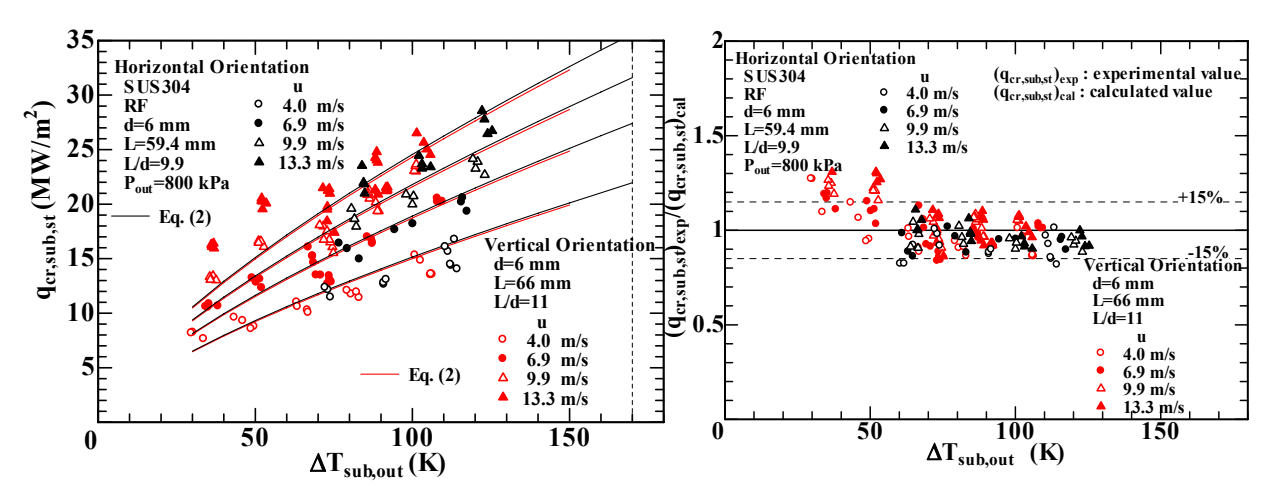


Fig. 11 $q_{cr,sub,st}$ vs. $\Delta T_{sub,out}$ for an inner diameter of 6mm with the heated length of 59.4 mm at an outlet pressure of around 800 kPa

Fig. 12 Ratio of CHF data for the inner diameter of 6 mm to the values derived from the outlet CHF correlation versus $\Delta T_{sub,out}$ at outlet pressure of around 800kPa

within ± 15 % difference for 4 m/s $\leq u \leq 13.3$ m/s and 29.7 K $\leq \Delta T_{sub,out} \leq 125.38$ K.

3.4.2 Inlet subcooling

It can be considered that the CHFs are determined not by the outlet conditions but by the inlet ones. The steady-state CHFs, $q_{cr,sub,st}$, for the HORIZONTAL SUS304 test tube of the inner diameter of 6 mm, L=59.4 mm, L/d=9.9 and δ =0.5 mm were shown versus the inlet subcooling, $\Delta T_{sub,in}$, with the flow velocities of 4 to 13.3 m/s in Fig. 13. The CHF data for the VERTICAL SUS304 test tube of d=6 mm, L=66 mm, L/d=11 and δ =0.5 mm with the flow velocities ranging from 4.0 to 13.3 m/s are also shown in the figure for comparison [24]. The $q_{cr,sub,st}$ for each flow velocity become higher with an increase in $\Delta T_{sub,in}$. The increasing rate becomes also lower for higher $\Delta T_{sub,in}$. The $q_{cr,sub,st}$ increase with an increase in the flow velocity at a fixed $\Delta T_{sub,in}$. The $q_{cr,sub,st}$ for the wide range of flow velocities are proportional to $\Delta T_{sub,in}$ for $\Delta T_{sub,in}$ >40 K.

The curves derived from Eq. (4) for the VERTICAL SUS304 test tube are shown in Fig. 13 for comparison. The CHF data for $\Delta T_{sub,in} \ge 40$ K are in good agreement with the values given by authors' correlation. To confirm the applicability of Eq. (4), the ratios of these CHF data for the d=6 mm HORIZONTAL test tube (69 points) and those for the d=6 mm VERTICAL one (110 points) to the corresponding values calculated by Eq. (4) are shown versus $\Delta T_{sub,in}$ in Fig. 14. Most of the data for $\Delta T_{sub,in} \ge 40$ K are within ± 15 % diffrence of Eq. (4) for the wide ranges of inlet subcoolings and flow velocities.

In this study, it is firmly confirmed that the transient CHF correlation against outlet and inlet subcoolings, Eqs. (2) and (4), can describe not only the authors' published CHF data (3137 points) for the VERTICAL SUS304 test tube within the wide ranges of inlet pressures (P_{in} =159 kPa to 1.1 MPa), inner diameters (d=2 to 12 mm), heated lengths (L=22 to 150 mm) and flow velocities (u=4.0 to 13.3 m/s) [23-38] but also the CHF data for the HORIZONTAL SUS304 test tube (69 points) obtained in this work on the inner diameter of 6 mm with L/d of 9.9 at the inlet pressure of 786.3 to 960.9 kPa within \pm 15 % difference for 30 K $\leq \Delta T_{sub,out} \leq$ 140 K and 40 K \leq

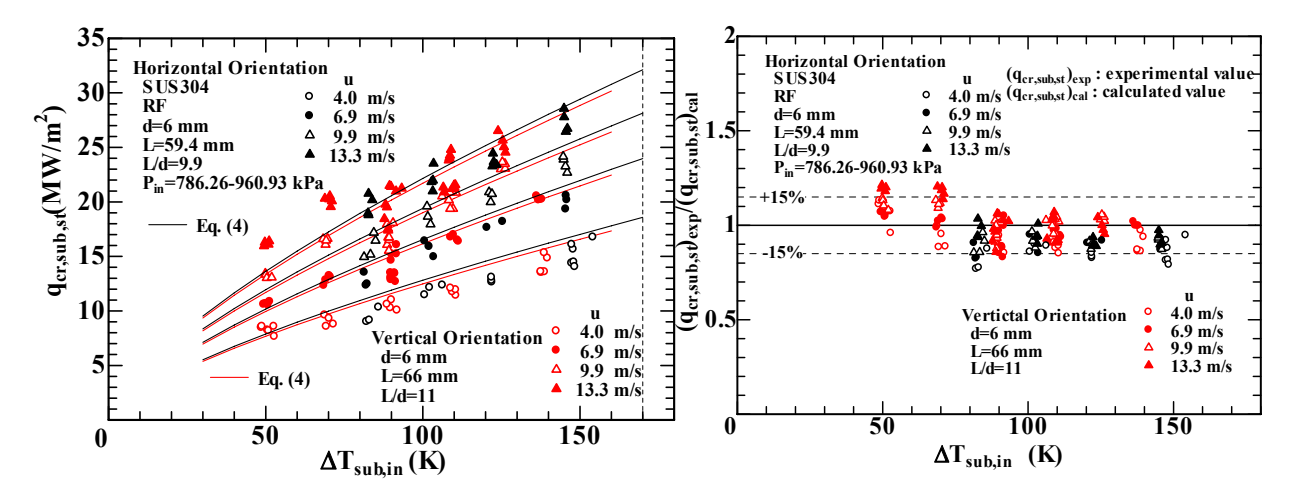


Fig. 13 Ratio of CHF data for the inner diameter of 6 mm to the values derived from the inlet CHF correlation versus $\Delta T_{sub,in}$ at the inlet pressures of 786.26 to 960.93 kPa

Fig. 14 Ratio of CHF data for the inner diameter of 6 mm to the values derived from the inlet CHF correlation versus $\Delta T_{sub,in}$ at the inlet pressures of 786.26 to 960.93 kPa

 $\Delta T_{sub,in} \le 151$ K. We have supposed that the expression of latent heat transport intensity at CHF point would be very useful to discuss the mechanism of the subcooled flow boiling critical heat flux, which would occur due to the hydro-dynamic instability suggested by Kutateladze [42] and Zuber [43] or due to the heterogeneous spontaneous nucleation at the lower limit of the heterogeneous spontaneous nucleation temperature [46]. The ratios of boiling number based on bubble motion to boiling number based on forced convection, Bo_{cr}/Bo_{con}, at the CHF surface superheat, $(\Delta T_{sat})_{cr}$, for the HORIZONTAL SUS304 test tube of d=6 mm and L=59.4 mm at inlet liquid temperatures (T_{in} =297.45 to 300.28 K) are shown versus u for the u ranging from 3.93 to 13.39 m/s in Fig. 15. Those for the VERTICAL SUS304 test tubes of d=3 mm and L=33 mm, and d=6 mm and L=59.5 mm with the rough finished inner surface at inlet liquid temperatures $(T_{in}=293.3 \text{ to } 316.2 \text{ K})$ are also shown versus u for the u ranging from 4.0 to 42 m/s in the figure as each red symbol for comparison [35,38]. These ratios on the log-log graph become linearly lower with an increase in the u. Those for the VERTICAL SUS304 tubes of d=3 and 6 mm with the rough finished inner surface become almost constant about 1 at the u higher than 40 m/s. The latent heat transport at CHF point would have almost disappeared, although the violent boiling noise was made for a period of time before the CHF point. The experimental data of Bo_{cr}/Bo_{con} for the HORIZONTAL SUS304 test tube of d=6 mm and those of Bo_{cr}/Bo_{con} for the VERTICAL SUS304 tubes of d=3 and 6 mm with the rough finished inner surface can be expressed for the uranging from 4 to 42 m/s by the following correlations: [35,38]

$$\frac{Bo_{cr}}{Bo_{con}} = 4.373u^{-0.4}$$
 for $u \le 40 \text{ m/s}$ (17)

$$\frac{Bo_{cr}}{Bo_{con}} = 1 for u > 40 \text{ m/s} (18)$$

It is assumed that the transition to film boiling at the u of 30 and 40 m/s would occur due to the heterogeneous spontaneous nucleation at the steady-state CHF but not due to the hydro-dynamic

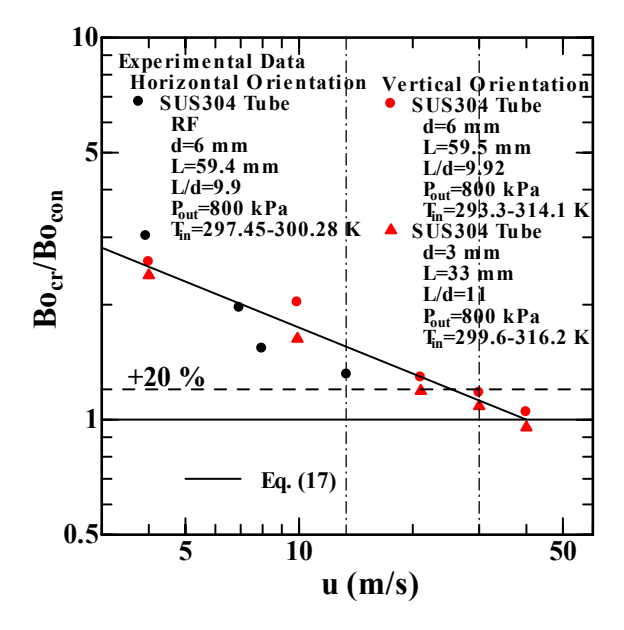


Fig. 15 Values of Bo_{cr}/Bo_{con} versus flow velocity for Horizontal SUS304 test tube of d=6 mm and Vertical SUS304 test tubes of d=3 and 6 mm

instability. The latent heat transport at CHF point has almost disappeared under the *u* higher than around 30 m/s and it would not be seen that the phenomenon occurs at some critical velocity in the vapor phase when the vapor jets start interfering with each other. It is the reason not to occur the hydrodynamic instability on the vapor-liquid interface at the CHF.

4. Conclusions

The steady-state turbulent heat transfer (THT) and the steady state nucleate boiling heat transfer (NBHT) and the steady state critical heat fluxes (CHFs) of the subcooled water flow boiling for HORIZONTAL Pt and SUS304 circular test tubes of the inner-diameter (d=6 mm), the heated lengths (L=69.6 and 59.5 mm), effective lengths (L=g=59.2 and 48.4 mm), L/d (=11.6 and 9.92) and L=g/d (=9.87 and 8.06) with surface roughness (R=0.45 and 3.89 μ m) were systematically measured for wide ranges of the flow velocities (u=3.93 to 13.86 m/s), the outlet subcoolings (ΔT _{sub,out}=60.40 to 142.75 K), the inlet subcoolings (ΔT _{sub,int}=81.30 to 154.20 K), the outlet pressures (P_{out}=773.41 to 972.00 kPa), the inlet pressures (P_{int}=786.29 to 960.93 kPa) and the exponentially increasing heat input (Q_{int} e=6.55 to 21.81 s). Experimental results lead to the following conclusions.

- 1) The heat flux gradually becomes higher with an increase in ΔT_L on the non-boiling forced convection curve derived from the correlation of the turbulent heat transfer for heating of water in a short vertical tube, Eq. (1). Equation (1) can describe the experimental data and the numerical solutions for the HORIZONTAL and VERTICAL test tubes within ± 15 % difference.
- 2) After the onset of nucleate boiling, the heat flux increases along the fully developed nucleate boiling curve up to the CHF at the u of 4 m/s. At the u higher than 6.9 m/s, the slope on the boiling curve does not increase with heat flux up to the CHF. The CHF and its surface superheat, ΔT_{sat} , become higher with an increase in flow velocity.
- 3) The fully developed nucleate boiling curves for the u of 4 m/s and the nucleate boiling curves in higher heat flux range for the u higher than 6.9 m/s can be almost described by Eqs. (11) and (12) within ± 15 % difference, respectively.
- 4) The value of *n* for the HORIZONTAL SUS304 test tube of *d*=6 mm is almost 1.5 at the *u* of 3.93 m/s. And those become linearly lower with an increase in the *u*. That becomes almost about 1.15 at the *u* of 13.39 m/s.
- 5) The $(\Delta T_{sat})_{cr}$ for HORIZONTAL SUS304 test tube become linearly higher with an increase in the flow velocity for the u ranging from 3.93 to 13.39 m/s, although those for the VERTICAL SUS304 test tubes of d=3 and 6 mm are almost constant $[(\Delta T_{sat})_{cr}=100 \text{ K}]$ for the u higher than 9.9 m/s.
- 6) Most of the steady state CHF data for HORIZONTAL SUS304 test tube of d=6 mm (69 points) are within ± 15 % differences of Eqs. (2) and (4) for the wide ranges of outlet subcoolings ($\Delta T_{sub,out}$ =60.40 to 142.75 K), inlet ones ($\Delta T_{sub,in}$ =81.30 to 154.20 K) and flow velocities (u=3.93 to 13.86 m/s).
- 7) The experimental data of Bo_{cr}/Bo_{con} for HORIZONTAL SUS304 test tube can be also expressed for the u ranging from 3.93 to 42 m/s by Eqs. (17) and (18).

5. Nomenclature

a, b, c fitted constant $Bo = q_{cr,sub}/Gh_{fg}$, boiling number (16/23)

```
C
          coefficient in Eq. (11)
                                                                    transient critical heat flux
                                                          q_{cr,sub}
C_1, C_2, C_3 constant in Eq. (4)
                                                                    subcooled condition, W/m<sup>2</sup>
                                                          q_{cr,sub,st} steady state critical heat flux, W/m<sup>2</sup>
C_4, C_5, C_6 constant in Eq. (5)
          specific heat, J/kg K
                                                          R_1 to R_3 resistance in a double bridge circuit,
           specific heat at constant pressure,
c_p
        J/kg K
                                                          Ra
                                                                   average roughness, µm
       =d/{\{\sigma/g/(\rho_l-\rho_g)\}}^{0.5}
D^*
                                  non-dimensional
                                                          Re
                                                                    =Gd/\mu_l, Reynolds number
       diameter
                                                                   maximum roughness depth, µm
                                                          Rmax
d
        test tube inner diameter, m
                                                                    resistance of the test tube, \Omega
                                                          R_T
G
        =\rho_l u, mass flux, kg/m<sup>2</sup>s
                                                          Rz
                                                                   mean roughness depth, um
        acceleration of gravity, m/s<sup>2</sup>
g
                                                                  initial exponential heat flux, W/m<sup>2</sup>
                                                          q_0
        latent heat of vaporization, J/kg
h_{fg}
                                                                  radial distance in cylindrical coordinate
       current flowing
                              through
                                           standard
                                                                  and test tube radius, m
       resistance, A
                                                                   test tube inner radius, m
                                                          r_i
Sc
          =c_{pl}(\Delta T_{sub,out})_{cal}/h_{fg}
                                   =c_{pl}\Delta T_{sub,out}/h_{fg}
                                                                   test tube outer radius, m
                                                          r_o
         non-dimensional outlet subcooling
                                                                    outer grid width for r-component
                                                          (\Delta r)_{out}
Sc*
          =c_{pl}\Delta T_{sub,in}/h_{fg}, non-dimensional inlet
                                                                   surface area, m<sup>2</sup>
                                                          S
          subcooling
                                                          T
                                                                   temperature of the test tube, K
        heated length, m
L
                                                           \overline{T}
                                                                   average temperature of the test tube, K
        entrance length, m
L_e
                                                          T_H
                                                                   homogeneous spontaneous nucleation
        effective length, m
L_{eff}
                                                                   temperature, K
          exit length, m
L_{ex}
                                                                   lower
                                                                              limit
                                                          T_{HET}
                                                                                        of
                                                                                               heterogeneous
          distance between
L_{ipt}
                                 inlet pressure
                                                                   spontaneous nucleation temperature,
         transducer and inlet of the heated
          section, m
                                                          T_{in}
                                                                   inlet liquid temperature, K
          distance between outlet pressure
L_{opt}
                                                          T_{out}
                                                                   outlet liquid temperature, K
         transducer and outlet of the heated
                                                                   inner surface temperature of the test
                                                          T_{s}
          section, m
                                                                   tube, K
          test section length, m
L_{ts}
                                                                    saturation temperature, K
                                                          T_{sat}
        =hd/\lambda_l, nusselt number
Nu_d
       exponent in Eq. (11)
                                                                   =\omega_p u/\{\sigma/g/(\rho_l-\rho_e)\}^{0.5}, non-dimensional
n
                                                          t^*
P
        pressure, kPa
                                                                   reduced time
       pressure at inlet of heated section, kPa
P_{in}
                                                                  reduced time for stepwise heat input, s
                                                          t_{cr}
         pressure measured by inlet pressure
P_{ipt}
                                                          t_{cr}/2 reduced time for ramp-wise heat input, s
         transducer, kPa
                                                          \Delta T_{sat}
                                                                    =T_s-T_{sat}, surface superheat, K
       pressure at outlet of heated section,
P_{out}
                                                          \Delta T_{sub,in}
                                                                    =(T_{sat}-T_{in}),
                                                                                          inlet
                                                                                                         liquid
                                                                     subcooling, K
P_{opt}
         pressure measured by outlet pressure
                                                          \Delta T_{sub.out} = (T_{sat} - T_{out}), outlet liquid subcooling,
         transducer, kPa
Pr
        =c_p\mu_l/\lambda_l, Prandtl number
                                                                   flow velocity, m/s
                                                          и
        heat input per unit volume, W/m<sup>3</sup>
Q
                                                          V
                                                                   volume, m<sup>3</sup>
Q_0
       initial exponential heat input, W/m<sup>3</sup>
                                                          V_I
                                                                   voltage
                                                                                                      standard
                                                                                drop
                                                                                          across
       step height of heat input per unit
Q_{s}
                                                                   resistance, V
       volume, W/m<sup>3</sup>
                                                          V_R
                                                                   voltage drop across two electrodes, V
        heat flux, W/m<sup>2</sup>
q
```

V_T	unbalance voltage in a double bridge	ω_p	reduced time, s
	circuit, V	•	
We	$=G^2d/\rho_l\sigma$, Weber number	Subscript	
Z	length, m		
\boldsymbol{z}	rectangular coordinate, m	cr	critical heat flux
α	coefficient of ramp heat input, W/m ³ s	g	vapor
δ	wall thickness, mm	in	inlet
θ	angle in cylindrical coordinate, radian	out	outlet
λ	thermal conductivity, W/mK	l	liquid
ρ	density, kg/m ³	sat	saturated conditions
σ	surface tension, N/m	sub	subcooled conditions
τ	exponential period, s	wnh	with no heating

6. Acknowledgments

This research was performed as a LHD joint research project of NIFS (National Institute for Fusion Science), Japan, NIFS05KFRF015, 2010. This research was supported by a Grant-in-Aid for Scientific Research from Japan Society for the Promotion of Science (22560196), 2010.

7. APPENDIX

7.1 Numerical solution of turbulent heat transfer [41]

7.1.1 Fundamental equations

The unsteady fundamental equations for turbulent heat transfer are expressed in the three dimensional coordinate shown in Fig. 16 as follows [48].

(Continuity Equation)

Cylindrical coordinates (r, θ, z) :

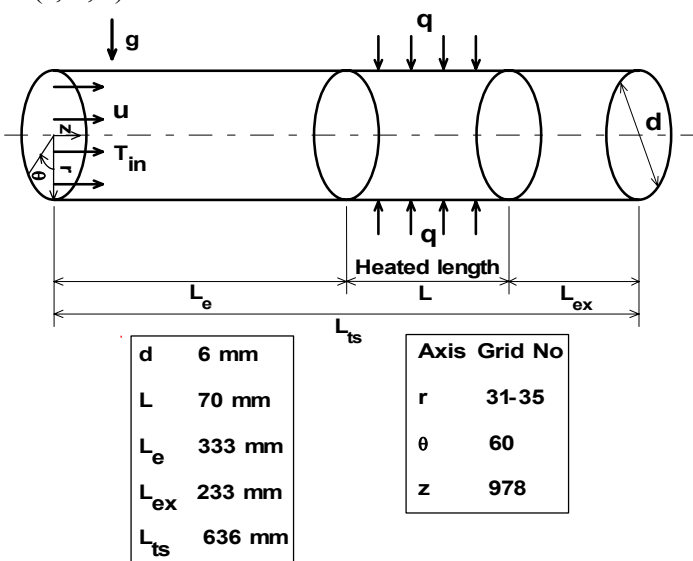


Fig. 16 Physical model for numerical analysis

$$\frac{\partial \rho}{\partial t} + \frac{1}{r} \frac{\partial}{\partial r} (\rho r v_r) + \frac{1}{r} \frac{\partial}{\partial \theta} (\rho v_\theta) + \frac{\partial}{\partial z} (\rho v_z) = 0 \tag{19}$$

(Momentum Equation)

r-component:

$$\rho \left(\frac{\partial v_r}{\partial t} + v_r \frac{\partial v_r}{\partial r} + \frac{v_\theta}{r} \frac{\partial v_r}{\partial \theta} - \frac{v_\theta^2}{r} + v_z \frac{\partial v_r}{\partial z} \right) = -\frac{\partial p}{\partial r} - \left(\frac{1}{r} \frac{\partial}{\partial r} (r \tau_{rr}) + \frac{1}{r} \frac{\partial \tau_{r\theta}}{\partial \theta} - \frac{\tau_{\theta\theta}}{r} + \frac{\partial \tau_{rz}}{\partial z} \right) + \rho g_r$$
 (20)

 θ -component:

$$\rho \left(\frac{\partial v_{\theta}}{\partial t} + v_{r} \frac{\partial v_{\theta}}{\partial r} + \frac{v_{\theta}}{r} \frac{\partial v_{\theta}}{\partial \theta} - \frac{v_{r}v_{\theta}}{r} + v_{z} \frac{\partial v_{\theta}}{\partial z} \right) = -\frac{1}{r} \frac{\partial p}{\partial \theta} - \left(\frac{1}{r^{2}} \frac{\partial}{\partial r} (r^{2} \tau_{r\theta}) + \frac{1}{r} \frac{\partial \tau_{\theta\theta}}{\partial \theta} + \frac{\partial \tau_{\theta z}}{\partial z} \right) + \rho g_{\theta}$$
(21)

z-component:

$$\rho \left(\frac{\partial v_z}{\partial t} + v_r \frac{\partial v_z}{\partial r} + \frac{v_\theta}{r} \frac{\partial v_z}{\partial \theta} + v_z \frac{\partial v_z}{\partial z} \right) = -\frac{\partial p}{\partial z} - \left(\frac{1}{r} \frac{\partial}{\partial r} (r \tau_{rz}) + \frac{1}{r} \frac{\partial \tau_{\theta z}}{\partial \theta} + \frac{\partial \tau_{zz}}{\partial z} \right) + \rho g_z$$
 (22)

(Energy Equation)

Cylindrical coordinates (r, θ, z) :

$$\rho c_{v} \left(\frac{\partial T}{\partial t} + v_{r} \frac{\partial T}{\partial r} + \frac{v_{\theta}}{r} \frac{\partial T}{\partial \theta} + v_{z} \frac{\partial T}{\partial z} \right) = - \left[\frac{1}{r} \frac{\partial}{\partial r} (rq_{r}) + \frac{1}{r} \frac{\partial q_{\theta}}{\partial \theta} + \frac{\partial q_{z}}{\partial z} \right]$$
(23)

where

$$\tau_{rr} = -\mu \left[2 \frac{\partial v_r}{\partial r} - \frac{2}{3} (\nabla \cdot v) \right] \tag{24}, \quad \tau_{\theta\theta} = -\mu \left[2 \left(\frac{1}{r} \frac{\partial v_{\theta}}{\partial \theta} + \frac{v_r}{r} \right) - \frac{2}{3} (\nabla \cdot v) \right]$$

$$\tau_{zz} = -\mu \left[2 \frac{\partial v_z}{\partial z} - \frac{2}{3} (\nabla \cdot v) \right]$$
 (26),
$$\tau_{r\theta} = \tau_{\theta r} = -\mu \left[r \frac{\partial}{\partial r} \left(\frac{v_{\theta}}{r} \right) + \frac{1}{r} \frac{\partial v_r}{\partial \theta} \right]$$
 (27)

$$\tau_{\theta z} = \tau_{z\theta} = -\mu \left[\frac{\partial v_{\theta}}{\partial z} + \frac{1}{r} \frac{\partial v_{z}}{\partial \theta} \right] \tag{28}, \quad \tau_{zr} = \tau_{rz} = -\mu \left[\frac{\partial v_{z}}{\partial r} + \frac{\partial v_{r}}{\partial z} \right]$$

$$(\nabla \cdot v) = \frac{\partial v_r}{\partial r} + \frac{1}{r} \frac{\partial v_\theta}{\partial \theta} + \frac{\partial v_z}{\partial z}$$
 (30)

 v_r , v_θ and v_z are the r, θ and z components of a velocity vector, respectively.

7.1.2 Boundary conditions

The fundamental equations are numerically analyzed together with the following boundary conditions. On the outer boundary of heated section: constant heat flux, and non-slip condition.

$$q = -\lambda \frac{\partial T}{\partial r} = cons \tan t \tag{31}$$

At the outer boundary of non-heated section:

$$\frac{\partial T}{\partial r} = \theta \tag{32}$$

At the lower boundary:

$$T = T_{in}$$
, $v_r = 0$, $v_{\theta} = 0$ and $v_z = u$ for in-flow,

where T_{in} and u are a inlet liquid temperature and a flow velocity at the entrance of the test section.

7.1.3 Method of solution

The control volume discretization equations were derived from these fundamental equations by using the hybrid scheme [49]. The thermo-physical properties for each control volume are given as those at each volume temperature. The procedure for the calculation of the flow field is the SIMPLE algorithm which stands for Semi-Implicit Method for Pressure-Linked Equations.

The surface heat fluxes, q, for the heated length were equally given in the range of 2.55×10^5 to 1.17×10^7 W/m² as an initial condition, and numerical calculation was continued until the steady-state was obtained. The surface temperature on the test tube, T_s , was calculated from the analyzed temperature of the outer control volume on the test tube surface, TEM, which is supposed to be located on the center of the control volume, by solving the heat conduction equation in liquid, $T_s = (\Delta r)_{out} q/2\lambda_l + TEM$. Average heat transfer coefficient on the test tube surface was obtained by averaging the calculated local surface temperatures at every 0.5 mm in the heated length, L. All the calculations were made by using the PHOENICS code [40].

8. References

- [1] Dittus, F., W., and Boelter, L., M., K., Univ. Calif. (Berkeley) Pub. Eng., Vol.2, (1930), p. 443.
- [2] Nusselt, W., Der Wärmeaustausch zweischen Wand und Wasser im Rohr, *Forsch. Geb. Ingenieurwes.*, Vol. 2, (1931), p. 309.
- [3] Sieder, E. N., and Tate, C. E., Heat Transfer and Pressure Drop of Liquids in Tubes, *Ind. Eng. Chem.*, Vol. 28, (1936), pp. 1429-1435.
- [4] Petukhov, B. S., Heat Transfer and Friction in Turbulent Pipe Flow with Variable Physical Properties, *Advances in Heat Transfer*, New York, Academic Press, (1970), pp. 503-564.
- [5] Gnielinski, V., New Equations for Heat and Mass Transfer in Turbulent Pipe and Channel Flow, *International Chemical Engineering*, Vol. 16, No. 2, (1976), pp. 359-368.
- [6] McAdams, W. H., Kennel, W. E., Minden, C. S. L., Carl, R., Picornell, P. M., and Dew, J. E., 1949, "Heat Transfer at High Rates to Water with Surface Boiling," Ind. Engng. Chem., 41, No.9, pp. 1945-1953.
- [7] Jens, W. H., and Lottes, P. A., 1951, "Analysis of Heat Transfer Burnout, Pressure Drop and Density Data for High Pressure Water," ANL-4627, May.
- [8] Rohsenow W. M., 1952, "A Method of Correlating Heat-Transfer Data for Surface Boiling of Liquids," Transactions of ASME, Vol. 74, pp. 969-976.
- [9] Thom, J. R. S., Walker, W. M., Fallon, T. A., and Reising, G. F. S., 1966, "Boiling in

- Subcooled Water during Flow up Heated Tubes or Annuli, Proc. Inst. Mech. Engrs," 180, Pt 3C, pp. 226-246.
- [10] Bergles, A.E., 1963, "Subcooled Burnout in Tubes of Small Diameter," ASME Paper No. 63-WA-182, pp. 1-9.
- [11] Nariai, H., Inasaka, F., and Shimura, T., 1987, "Critical Heat Flux of Subcooled Flow Boiling in Narrow Tube," Proceedings of the 1987 ASME-JSME Thermal Engineering Joint Conference, 5, Hemisphere, New York, pp. 455-462.
- [12] Celata, G.P., Cumo, M., and Mariani, A., 1992, "Subcooled Water Flow Boiling CHF with Very High Heat Fluxes," Revue Generale de Thermique, **n'362**, pp. 29-37.
- [13] Celata, G.P., Cumo, M., and Mariani A., 1994, "Enhancement of CHF Water Subcooled Flow Boiling in Tubes using Helically Coiled Wires," *International Journal of Heat and Mass Transfer*, **37**(1), pp. 53-67.
- [14] Celata, G.P., 1998, "Critical Heat Flux in Subcooled Flow Boiling," Heat Transfer 1998, Proceedings of 11th International Heat Transfer Conference, 1, pp. 261-277.
- [15] Vandervort, C.L., Bergles, A.E., and Jensen, M.K., 1994, "An Experiment Study of Critical Heat Flux in Very High Heat Flux Subcooled Boiling," *International Journal of Heat and Mass Transfer*, **37**, Suppl. 1, pp. 161-173.
- [16] Mudawar, I., and Bowers, M.B., 1999, "Ultra-high Critical Heat Flux (CHF) for Subcooled Water Flow Boiling-I: CHF data and parametric effects for small diameter tubes," *International Journal of Heat and Mass Transfer*, **42**, pp. 1405-1428.
- [17] Kataoka, I., Serizawa, A., and Sakurai, A., 1983, "Transient Boiling Heat Transfer under Forced Convection," *International Journal of Heat and Mass Transfer*, **26**, No. 4, pp. 583-595.
- [18] Celata, G. P., Cumo, M., D'Annibale, F., Farello, G. E., and Said, S. A., 1988, "Critical Heat Flux Phenomena during Power Transients," *Heat and Technology*, **6**, No. 1-2, pp. 38-69.
- [19] Celata, G. P., Cumo, M., D'Annibale, F., and Farello, G. E., 1989, "Critical Heat Flux in Transient Flow Boiling during Simultaneous Variations in Flow Rate and Thermal Power," *Experimental Thermal and Fluid Science*, **2**, No. 2, pp. 134-145.
- [20] Celata, G. P., Cumo, M., and D'Annibale, F., 1992, "A Data Set of Critical Heat Flux of Boiling R-12 in Uniformly Heated Vertical Tubes under Transient Conditions," *Experimental Thermal and Fluid Science*, **5**, No. 1, pp. 78-107.
- [21] Sawan, M. E., and Santoro, R. T., 1998, "Nuclear Heating and Damage Profiles in the ITER Divertor Cassette," Fusion Engineering, 1977. 17th IEEE/NPSS Symposium, **2**, pp. 833-836.
- [22] Hata, K., and Noda, N., 2008, "Turbulent Heat Transfer for Heating of Water in a Short Vertical Tube," *Journal of Power and Energy Systems*, **2**, No. 1, pp. 318-329.
- [23] Hata, K., Shiotsu, M., and Noda, N., 2004, "Critical Heat Fluxes of Subcooled Water Flow Boiling against Outlet Subcooling in Short Vertical Tube," *Journal of Heat Transfer*, Trans. ASME, Series C, **126**, pp. 312-320.
- [24] Hata, K., Komori, H., Shiotsu, M., and Noda, N., 2004, "Critical Heat Fluxes of Subcooled Water Flow Boiling against Inlet Subcooling in Short Vertical Tube," *JSME International Journal*, Series B, 47, No. 2, pp. 306-315.
- [25] Hata, K., Komori, H., Shiotsu, M., and Noda, N., 2004, "Influence of Dissolved Gas Concentration on Subcooled Flow Boiling Critical Heat Flux in Short Vertical Tube," *Proceedings of 12th International Conference on Nuclear Engineering*, Paper No. ICONE12-49194, pp. 1-11.
- [26] Hata, K., Shiotsu, M., and Noda, N., 2004, "Subcooled Flow Boiling Critical Heat Flux

- in Short Vertical Tube (Influence of Inner Surface Roughness)," *Proceedings of 2004 ASME International Mechanical Engineering Congress and RD&D Expo*, Paper No. IMECE2004-61453, pp. 1-10.
- [27] Hata, K., and Noda, N., 2005, "Subcooled flow boiling heat transfer and critical heat flux in short vertical tube with mirror finished inner surface," *Proceedings of 11th International Topical Meeting on Nuclear Reactor Thermal Hydraulics*, Paper No. NURETH11-281, pp. 1-20.
- [28] Hata, K., and Noda, N., 2006, "Thermal Analysis on Flat-Plate Type Divertor Based on Subcooled Flow Boiling Critical Heat Flux Data against Inlet Subcooling in Short Vertical Tube," *Journal of Heat Transfer*, Trans. ASME, Series C, **128**, pp. 311-317.
- [29] Hata, K., Shiotsu, M., and Noda, N., 2006, "Thermal Analysis on Mono-Block Type Divertor Based on Subcooled Flow Boiling Critical Heat Flux Data against Inlet Subcooling in Short Vertical Tube," *Plasma and Fusion Research*, **1**, No. 017, pp. 1-10.
- [30] Hata, K., Shiotsu, M., and Noda, N., 2006, "Critical Heat Flux of Subcooled Water Flow Boiling for High *L/d* Region," *Nuclear Science and Engineering*, **154**, No. 1, pp. 94-109.
- [31] Hata, K., Shiotsu, M., and Noda, N., 2006, "Influence of Heating Rate on Subcooled Flow Boiling Critical Heat Flux in a Short Vertical Tube," *JSME International Journal*, Series B, **49**, No. 2, pp. 309-317.
- [32] Hata, K., Shiotsu, M., and Noda, N., 2007, "Influence of Test Tube Material on Subcooled Flow Boiling Critical Heat Flux in Short Vertical Tube," *Journal of Power and Energy Systems*, 1, No. 1, pp. 49-63.
- [33] Hata, K., and Noda, N., 2008, "Turbulent Heat Transfer for Heating of Water in a Short Vertical Tube," *Journal of Power and Energy Systems*, **2**, No. 1, pp. 318-329.
- [34] Hata, K., and Noda, N., 2008, "Transient Critical Heat Fluxes of Subcooled Water Flow Boiling in a Short Vertical Tube Caused by Exponentially Increasing Heat Inputs," *Journal of Heat Transfer*, Trans. ASME, Series C, **130**, pp. 054503-1-9.
- [35] Hata, K., and Masuzaki, S., 2009, "Subcooled Boiling Heat Transfer in a Short Vertical SUS304-Tube at Liquid Reynolds Number Range 5.19×10⁴ to 7.43×10⁵," *Nuclear Engineering and Design*, **239**, pp. 2885-2907.
- [36] Hata, K., and Masuzaki, S., 2010, "Subcooled Boiling Heat Transfer for Turbulent Flow of Water in a Short Vertical Tube," *Journal of Heat Transfer*, Trans. ASME, Series C, **132**, pp. 011501-1-11.
- [37] Hata, K., and Masuzaki, S., 2010, "Influence of Heat Input Waveform on Transient Critical Heat Flux of Subcooled Water Flow Boiling in a Short Vertical Tube," *Nuclear Engineering and Design*, **240**, pp. 440-452.
- [38] Hata, K., and Masuzaki, S., "Critical Heat Fluxes of Subcooled Water Flow Boiling in a Short Vertical Tube at High Liquid Reynolds Number," *Nuclear Engineering and Design*, **240**, 2010, pp. 3145-3157.
- [39] Brodkey, R. S., and Hershey, H. C., 1988, *Transport Phenomena*, McGraw-Hill, New York, p. 568.
- [40] Spalding, D.B., 1991, *The PHOENICS Beginner's Guide*, CHAM Ltd., London, United Kingdom.
- [41] Hata, K., Kai, N., Shirai, Y., Masuzaki, S., and Hamura, A., 2011, "Computational Study of Turbulent Heat Transfer for Heating of Water in a Short Vertical Tube," *Proceedings of 19th International Conference on Nuclear Engineering*, Paper No. ICONE19-43301, pp. 1-11.
- [42] Kutateladze, S.S., 1959, "Heat Transfer in Condensation and Boiling," AEC-tr-3770,

USAEC.

- [43] Zuber, N., 1959, "Hydrodynamic Aspects of Boiling Heat Transfer," AECU-4439, USAEC.
- [44] Bergles, A. E., and Rohsenow, W.M., 1964, "The Determination of Forced-Convection Surface-Boiling Heat Transfer," *Journal of Heat Transfer*, Trans. ASME, Series C, **86**, pp. 365-372.
- [45] Rohsenow, W. M., 1952, "A Method of Correlating Heat-Transfer Data for Surface Boiling of Liquids," Transactions of ASME, 74, pp. 969-976.
- [46] Cole, C., 1979, "Homogeneous and heterogeneous nucleation in Boiling Phenomena," Vol. 1, Stralen, S. van, and Cole, R. eds., Hemisphere Pub. Corp., p. 71.
- [47] Lienhard, J. H., 1976, "Correlation of Limiting Liquid Superheat," *Chem. Eng. Science*, **31**, pp. 847-849.
- [48] Bird, R.B., Stewart, W.E., and Lightfoot, E.N., 1960, *Transport Phenomena*, New York, John Wiley & Sons, p. 85.
- [49] Patankar, S.V., 1980, *Numerical Heat Transfer and Fluid Flow*, Hemisphere Pub. Corp., New York.